GEOLOGY | THE GEOLOGICAL SOCIETY OF AMERICA®

https://doi.org/10.1130/G47115.1

Manuscript received 18 October 2019
Revised manuscript received 31 March 2020
Manuscript accepted 6 April 2020

Published online XX Month 2020

Experimental evidence for crustal control over seismic fault segmentation

M. Lefevre[1]*, P. Souloumiac[2], N. Cubas[3] and Y. Klinger[1]*
[1]Institut de Physique du Globe de Paris, Université de Paris, CNRS, 75005 Paris, France
[2]Laboratoire Géosciences et Environnement Cergy (GEC), CY Cergy Paris Université, F-95000 Cergy, France
[3]Institut des Sciences de la Terre de Paris (ISTeP), Sorbonne Université, 75005 Paris, France

ABSTRACT

Strike-slip faults are generally described as continuous structures, while they are actually formed of successive segments separated by geometrical complexities. Although this along-strike segmentation is known to affect the overall dynamics of earthquakes, the physical processes governing the scale of this segmentation remain unclear. Here, we use analogue models to investigate the structural development of strike-slip faults and the physical parameters controlling segmentation. We show that the length of fault segments is regular along strike and scales linearly with the thickness of the brittle material. Variations of the rheological properties only have minor effects on the scaling relationship. Ratios between the segment length and the brittle material thickness are similar for coseismic ruptures and sandbox experiments. This supports a model where crustal seismogenic thickness controls fault geometry. Finally, we show that the geometrical complexity acquired during strike-slip fault formation withstands cumulative displacement. Thus, the inherited complexity impedes the formation of an ever-straighter fault, and might control the length of earthquake ruptures.

INTRODUCTION

Strike-slip faults are discontinuous features formed by a succession of segments, separated by geometrical complexities such as bends or relay zones (Fig. 1A; Fig. S1 in the Supplemental Material[1]) (e.g., Segall and Pollard, 1980). Although the size of these complexities is highly variable, even the smaller ones can significantly affect the initiation, propagation, and termination of earthquakes (e.g., King and Nábělek, 1985; Klinger et al., 2005; Wesnousky, 2006; Manighetti et al., 2007), implying their persistence at seismogenic depth (e.g., Schwartz and Coppersmith, 1984; Wei et al., 2011; Schwartz, 2018). Fault discontinuities also modulate the amplitude and style of coseismic surface deformation (Klinger et al., 2006; Vallée et al., 2008), and might stop rupture propagation if longer than 5 km (e.g., Wesnousky, 2006). Recently, numerical simulations of rupture scenarios have confirmed the strong dependency of earthquake rupture models on the geometry of the fault system (e.g., Aochi and Ulrich, 2015; Lozos, 2016; Klinger et al., 2018). As a consequence, understanding the genesis of the segmentation and its scaling is critical for physics-based earthquake modeling as well as for hazard assessment, since complexities impact the earthquake rupture length and thus its magnitude.

Based on experimental, seismological, and geomorphological studies, fault segmentation was first described as fractal (e.g., Aviles et al., 1987; Okubo and Aki, 1987). Alternatively, it has been suggested from fluctuations of the cumulative slip along strike that faults are composed of a fixed number of segments, implying a segment length varying between faults (e.g., Manighetti et al., 2015).

Conversely, studies based on coseismic rupture maps have argued in favor of a constant segment length of ~18 ± 5 km, independent of the regional tectonic setting or the earthquake magnitude, suggesting an external controlling factor, which is assumed to be the seismogenic crust thickness (e.g., Bilham and Williams, 1985; Klinger, 2010) (Fig. 1A). However, detailed coseismic rupture maps are available for only a limited number of earthquakes, preventing a reliable statistical analysis. The lack of data combined with our limited knowledge of the fault segmentation process prevent us from discriminating between these models.

To tackle the origin of strike-slip fault segmentation, we followed an analogue modeling approach, which provides the complete geometrical evolution of the fault structure while accumulating slip. Moreover, a large number of experiments can be conducted, allowing for a thorough exploration of the impact of the geometrical and rheological parameters.

ANALOGUE MODELING OF STRIKE-SLIP FAULTS

Numerous analogue studies have already focused on the formation and final geometry of strike-slip fault systems (Dooley and Schreurs, 2012, and references therein). In experiments with sand overlying a straight basal dislocation, the first structures to appear are the Riedel shears (R-shears) (Riedel, 1929; Naylor et al., 1986), propagating upward (e.g., Ueta et al., 2000; Cambonie et al., 2019), oriented at the surface at an angle of $\varphi_{int}/2$ relative to strike-slip basal fault (where φ_{int} is the angle of internal friction of the material). This orientation is due to the helicoidal shape of the Riedel shears (Fig. 1B) (Naylor et al., 1986; Mandl, 1987). The next structures to appear are, first, synthetic shears (S-shears) that only slightly deviate from the strike of the basal fault, and finally P-shears, which cross the basal fault in the opposite direction. Eventually, coalescence of these different

*E-mails: marthe.lefevre1@gmail.com; klinger@ipgp.fr

[1]Supplemental Material. Experimental set-up, model validation, materials properties, experiment results, and seismogenic thickness values. Please visit https://doi.org/10.1130/XXXXX to access the supplemental material, and contact editing@geosociety.org with any questions.

CITATION: Lefevre, M., Souloumiac, P., Cubas, N., and Klinger, Y., 2020, Experimental evidence for crustal control over seismic fault segmentation: Geology, v. 48, p. XXX–XXX, https://doi.org/10.1130/G47115.1

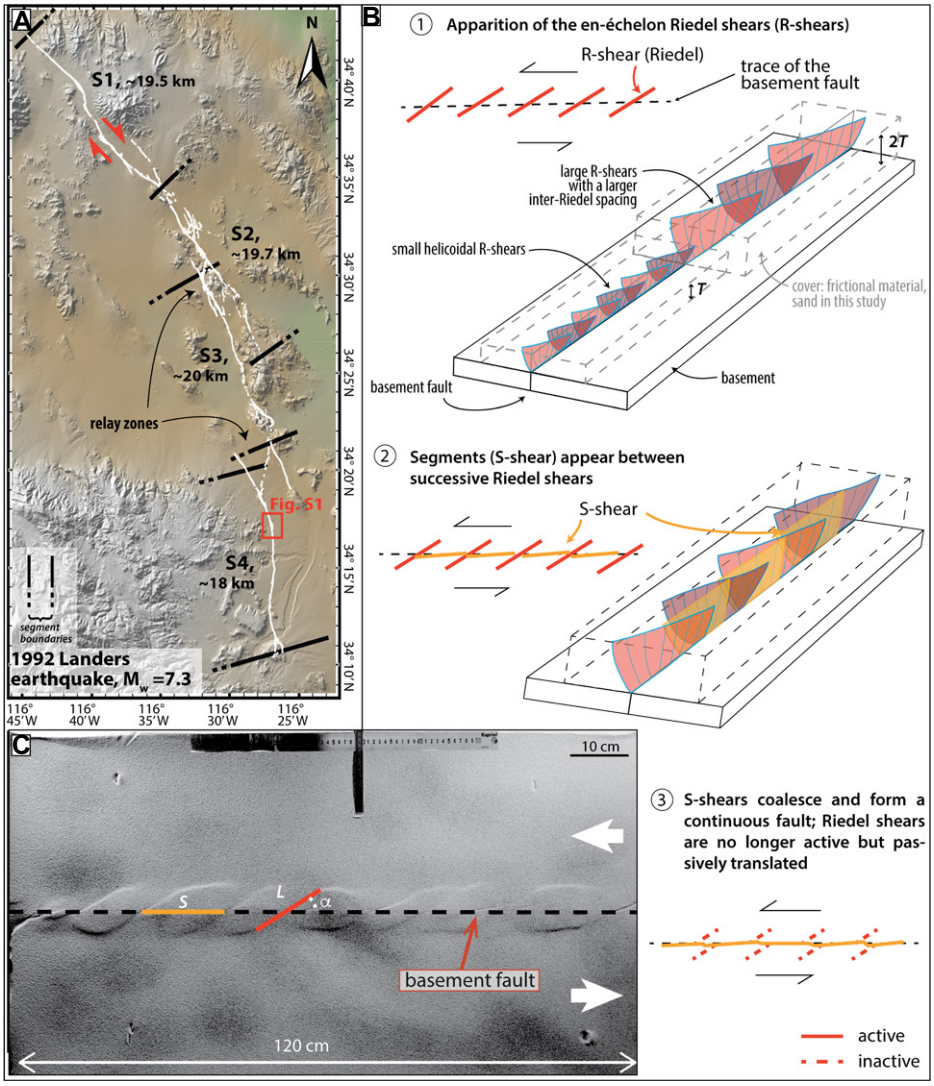

Figure 1. (A) Surface rupture map of the 1992 CE Landers earthquake, California (USA). Segmentation (black lines) is according to Klinger (2010). Red box shows area of Figure S1 in the Supplemental Material (see footnote 1). (B) Evolutionary scheme of formation of strike-slip faults, seen from the surface, and three-dimensional sketch to illustrate helicoidal shape of Riedel shears. (C) Top view of experiment sandbox, with measured parameters: *S*—inter-Riedel distance; *L*—Riedel shear length; α—angle between Riedel shear and basement fault.

shears leads to the formation of an anastomosed fault zone (e.g., Naylor et al., 1986; Richard et al., 1995).

Here, we investigate whether the first structures to appear during the formation of strike-slip faults can be responsible for the long-term segmentation. As these faults result from the linkage of the S-shears, the initial discontinuities between them at the locations of the Riedel shears might persist and give rise to geometrical complexities. Therefore, we consider the distance between two adjacent Riedel shears as equivalent to a fault segment. Although dependency of the length of Riedel shears on the thickness of the frictional material had already been suspected, it has never been indisputably demonstrated (Tchalenko, 1970; Atmaoui et al., 2006; Hatem et al., 2017). Thus, we first evaluate the influence of the material thickness on the inter-Riedel distance, and then the impact of intrinsic properties of the material.

We used an analogue model setup known as the Riedel experiment in a 1.2 m × 0.8 m box (detailed setup is shown in Fig. S2 in the Supplemental Material). The model reproduces brittle deformation in a noncohesive material during the onset of a strike-slip fault in a homogeneous sand pack above a straight-basal fault. To test the impact of frictional properties on the fault geometry, we used four different eolian sands with different angles of internal friction (Sand 1, $\varphi_{int} = 43.7°$; Sand 2, $\varphi_{int} = 35.6°$; Sand 3, $\varphi_{int} = 33.4°$; Sand 4, $\varphi_{int} = 22.1°$) and variable basal materials such as PVC ($\varphi_b = 13°$; φ_b—angle of basal friction), Alkor-foil ($\varphi_b = 18°$), and sandpaper ($\varphi_b > 43.7°$). Some of the sands were poured and had a rate-hardening behavior (Sands 2, 3, and 4), while Sand 1 was sedimented and rate weakening (see the Supplemental Material for material properties). A camera placed above the box recorded the deformation every 0.5 mm of basal displacement to generate orthoimages of the sandbox surface, with a resolution of the order of the grain size. Moreover, to assess how the shear is accommodated by the different structures, we computed the incremental displacement field from optical image correlation using MicMac software (Rosu et al., 2015). The setup is intentionally simple to limit the number of parameters and to ensure a good control on the boundary conditions of the experiment. The aim of these experiments is not to reproduce details of a realistic strike-slip fault evolution, but to retrieve relationships between fault-characteristic patterns and properties of material.

For each sand-pack thickness (*T*), three parameters were extracted from surface images for each R-shear: the inter-Riedel distance (*S*) measured parallel to the trace of the basal fault, the Riedel shear length (*L*), and the angle (α) formed by the R-shear with the direction of the basal fault (Fig. 1C). We ran repeated experiments with thicknesses varying from 2 to 5 cm (Table S1 in the Supplemental Material). Only the experiments with thicknesses less than or equal to 5 cm were free of edge effects (Fig. S3). The minimum thickness is constrained by the ability of the sand to develop the three-dimensional helicoidal shape of Riedel shears. For thicknesses less than 1.5 cm, instead of the Riedel shears, a continuous fault appears directly at the surface (Fig. S4).

To provide robust correlations between thickness, material properties, and fault geometry, we need repeated experimental measurements. As several Riedel shears are visible in each experiment, we checked that we could use them as independent measurements to improve statistical significance (see verification in the Supplemental Material). In the following, for clarity's sake, only average quantities per experiment are presented and discussed (individual measurements are presented in Figs. S7–S11).

SCALING RELATIONSHIPS DERIVED FROM SANDBOX EXPERIMENTS

Surface images of the experiments for different thicknesses (*T*) show that the deformed area widens and the inter-Riedel distance (*S*) increases for thicker sand packs (Fig. 2A). Indeed, systematic measurements of *S* for different *T* show a linear correlation between those parameters (Fig. 2B), with a scale factor of ~2.8 for Sand 1.

To test the potential effect of the material properties, we first performed experiments using sands with different angles of internal friction. The three sets of experiments exhibit the same trend: *S* increases with *T* (Fig. 2C; Fig. S7), and the measurement distributions are well modeled

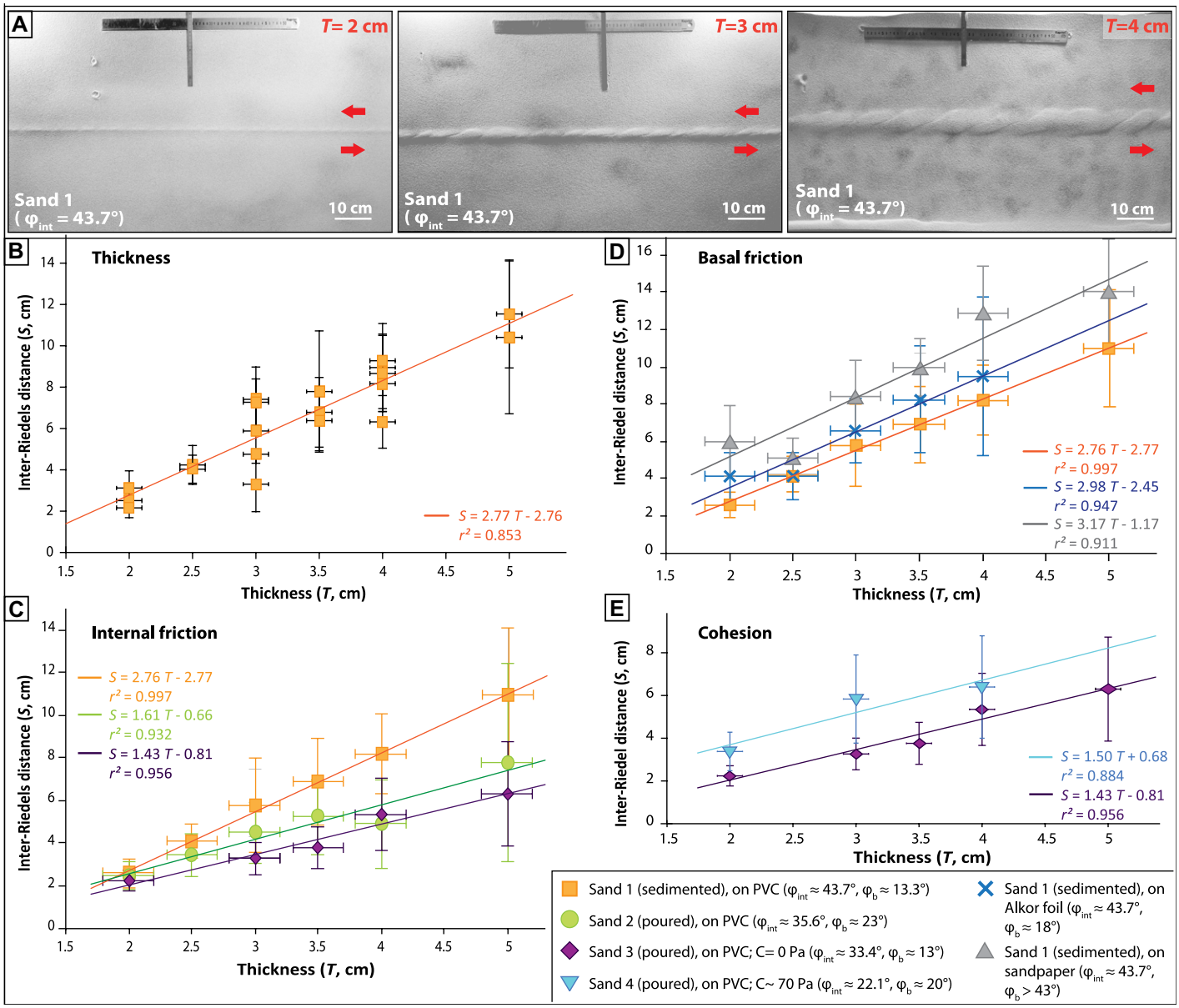

Figure 2. Comparison between inter-Riedel distance (*S*) and sand-pack thickness (*T*) for different frictional and cohesional properties of sand. (A) Photos of the top of the sandbox after ~11–12 mm of displacement for experiments with 2-, 3-, and 4-cm-thick sand pack. (B–E) Average inter-Riedel distance (*S*) per experiment versus sand-pack thickness (*T*) for Sand 1 (B); for three different sands with different angles of internal friction (φ_{int}) (C); for three different basal materials to study basal friction effect (φ_b—angle of basal friction) (D); and for two sands with different cohesion (C—cohesion) (E). Error bars represent the standard deviations of the measurements for each experiment. Note that for clarity's sake, for Sand 1 in C and D, we represent average value by thickness rather than by experiment.

by linear relationships. Nevertheless, depending on the angle of internal friction, the slope of the best-fit lines changes, indicating a partial control of the material properties on the size of the structures. The slope is 1.43 for the smaller angle of friction (φ_{int} = 33.4°, Sand 3), 1.61 for the intermediate angle of friction (φ_{int} = 35.6°, Sand 2), and 2.76 for the highest one (φ_{int} = 43.7°, Sand 1). Because Sands 2 and 3 present relatively similar relationships (Fig. 2C) and are both strain hardening, we cannot exclude from our data that the discrepancy between Sand 1 and the other sands could be due to its strain-weakening properties instead of its angle of internal friction (Fig. S11). Nevertheless, as Riedel shears form when shear stress reaches the static friction, as confirmed by α angles (Tchalenko, 1970; Ritter et al., 2018; Fig. S10), we think that the internal friction of the sands controls the relation between *S* and *T*, and not its strain-hardening or strain-weakening property.

Using different materials to test the impact of the internal friction might also change the basal friction between the different experiments. To assess a possible tradeoff between these two parameters, we conducted three series of experiments using Sand 1 with different basal materials (Fig. 2D; Fig. S7). For the three tested basal frictions, we observed linear relations between *S* and *T*. The slopes of the regressions are quite similar, and only the intercepts change slightly (Fig. 2D). The associated change of *x*-axis intercept corresponds to the minimal thickness necessary to develop the Riedel helicoid. This observation suggests that the basal friction impacts the formation of the helicoid, probably by changing the width of the deformed area at depth (see the Supplemental Material for mechanical implications).

We then examined the effect of the cohesion on the inter-Riedel distance (*S*), using noncohesive (Sand 3) and strongly cohesive (Sand 4) sands (Fig. 2E; Fig. S8). Again, *S* increases linearly with *T*. The two linear regressions present the same slope but shifted intercepts, with

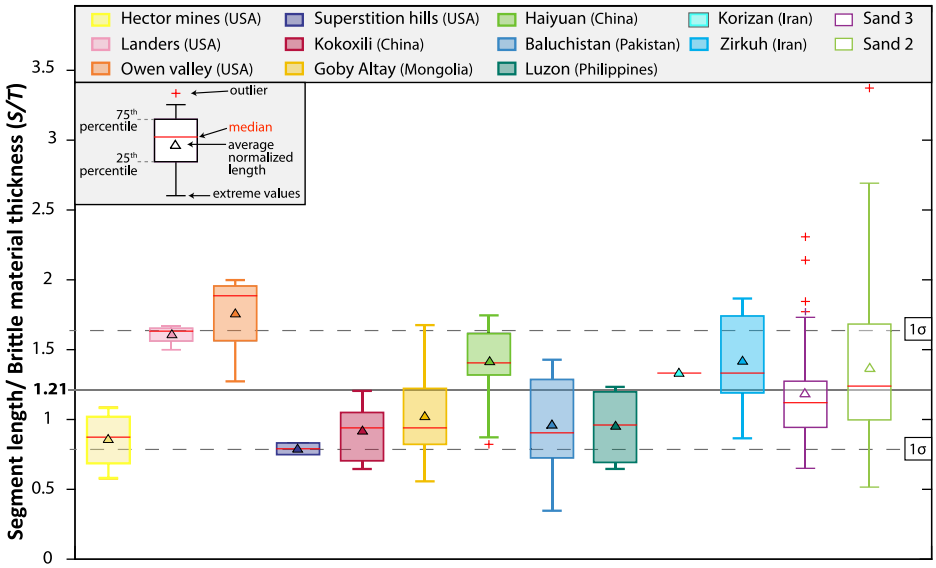

Figure 3. Normalized length of individual fault segments for several continental strike-slip earthquakes (Klinger, 2010; Lauer et al., 2018) and for individual analogue-fault segments (Sands 2 and Sand 3; see Fig. S13 [see footnote 1] for comparison with Sands 1 and 4). Lengths are normalized by inferred seismogenic thickness, which are estimated from the literature (see the Supplemental Material [see footnote 1]), or by sand thickness accordingly. The average value of the *S*/*T* ratio (*S*—inter-Riedel distance; *T*—sand-pack thickness) for both datasets is 1.21, and the standard deviation is indicated by the dashed lines.

a larger value for the highly cohesive sand (of ~1.5 cm). However, this difference may not be significant in view of the small number of experiments associated with a high dispersion of the Sand 4 measurements, interpreted as resulting from heterogeneities in the sand mixture due to its electrostatic charge (see the Supplemental Material). We consider that cohesion only marginally affects the fault geometry because *S* is only slightly affected whereas all other parameters vary and uncertainties are significant.

COMPARISON OF EXPERIMENTAL RESULTS WITH EARTHQUAKE SURFACE RUPTURE GEOMETRY

This new set of experiments demonstrates unambiguously that the inter-Riedel distance (*S*) is directly controlled by the thickness of the sand pack (*T*) (Fig. 2), while the material properties have secondary effects. The internal friction of the sand controls the scaling factor of the linear relation between *S* and *T*, whereas its basal friction and cohesion only marginally impact this relation. The width and rheology of the basal deformation zone, which are not addressed here, might also affect the size of structures (Hatem et al., 2017; Zuza et al., 2017; Yang et al., 2020).

According to field studies, strike-slip fault segments, measured between two successive relay zones, have similar lengths independently of the local tectonic setting (Klinger, 2010). Thus, it has been suggested that the average length of fault segments scales with the thickness of the seismogenic crust (Bilham and Williams, 1985; Klinger, 2010), with a ratio close to 1. To compare our experiments with natural observations, we selected Sands 2 and 3, both non-dilatant and with coefficients of friction within the same range as standard upper-crust materials (μ ~0.7) (e.g., Byerlee, 1978).

For comparison, the inter-Riedel distance and the length of fault segments were normalized respectively by the thickness of sand and of seismogenic crust, which is derived from the literature (see details in the Supplemental Material). The average normalized length for natural fault segments is 1.16, while for Sands 2 and 3 it is 1.17 and 1.3, respectively, which are indistinguishable from the value for natural cases (Fig. 3). Moreover, individual *S*/*T* ratio values are all in a narrow range (σ = 0.43), which indicates that such similarity is not coincidental. This supports the hypothesis that the length of continental strike-slip segments is directly controlled by the thickness of the seismogenic crust.

Although this approach does not capture the effects of a dynamic rupture, it sheds light upon the way fault sections grow to eventually coalesce into an apparent continuous structure. Interestingly, our experiments show that even when the cumulative displacement during the experiment starts to be large enough to dismantle the Riedel shears and to allow coalescence of successive S-shears into a longer fault, the initial geometric discontinuity related to the location of a Riedel shear is preserved (Fig. 4A). Riedel shears act as inherited faults, influencing the location of subsequent deformation. In the case of strike-slip faults, such discontinuities turn into relay zones, either compressional or extensional. Indeed, in nature, faults form in crust that has already undergone multiple stages of deformation and that displays local geological variation. Thus the simple scenario of faults structured only according to the thickness of the brittle crust is likely modulated by inherited crustal heterogeneities, resulting in some relay zones being larger than others. Sandbox experiments can also present such variability with larger complexities randomly appearing (Fig. S14), suggesting that the initial orientation

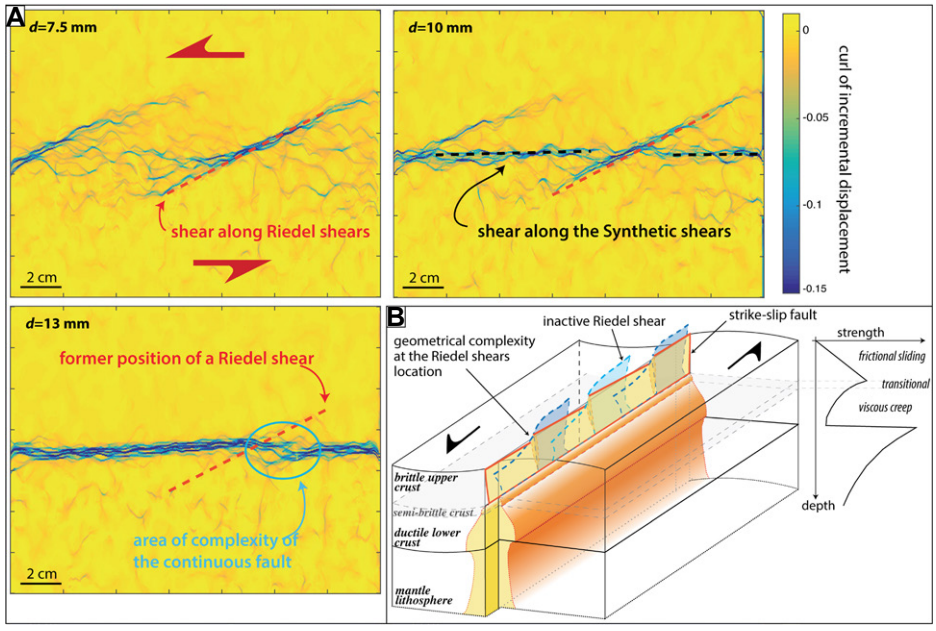

Figure 4. (A) Curl of incremental displacement field at three different stages of deformation (*d* = 7.5 mm, *d* = 10 mm, *d* = 13 mm) for an experiment with a 4-cm-thick sand-pack. Curl is derived from correlation image between two successive pictures of sandbox surface; it highlights location of shear. Location of different active faults (Riedel and synthetic shears) is highlighted. (B) Three-dimensional scheme of structures of strike-slip fault at crustal scale.

of the S-shears might also influence the size of the relay zones. Other studies have proposed that off-fault deformation of earthquakes could be related to the reactivation of these Riedel shears (Hatem et al., 2017), although we could not observe such reactivation in our experiments. Moreover, in nature, evidence of the initial Riedel structures is tenuous, because they accommodate a very short amount of deformation before being passively offset by the main active fault, which explains their weak morphological expression at the surface.

These results show that the first stages of deformation determine the long-term scaling of strike-slip fault segmentation: Riedel shears create a regular pattern of geometrical complexities, which is inherited throughout the fault history (Fig. 4B). This pattern of segmentation does not seem to experience significant changes even after the Riedel shears have ceased to be active, given that we keep seeing it on coseismic-rupture maps. Thus, this questions the paradigm that faults become ever more linear while accumulating displacement through time, and thus prone to larger earthquakes. Instead, strike-slip fault geometry may retain a constant level of complexity, which controls the size of earthquakes.

ACKNOWLEDGMENTS

We thank Bertrand Maillot for his insights during experiments and result analyses. M. Cook, H. Yang, and an anonymous reviewer helped significantly improve this manuscript. This work has been partly funded by Agence Nationale de la Recherche (ANR, France) project GeoSMEC (ANR-12-BS06-0016). This is Institut de Physique du Globe de Paris contribution #4134.

REFERENCES CITED

Aochi, H., and Ulrich, T., 2015, A probable earthquake scenario near Istanbul determined from dynamic simulations: Bulletin of the Seismological Society of America, v. 105, p. 1468–1475, https://doi.org/10.1785/0120140283.

Atmaoui, N., Kukowski, N., Stöckhert, B., and König, D., 2006, Initiation and development of pull-apart basins with Riedel shear mechanism: Insights from scaled clay experiments: International Journal of Earth Sciences, v. 95, p. 225–238, https://doi.org/10.1007/s00531-005-0030-1.

Aviles, C.A., Scholz, C.H., and Boatwright, J., 1987, Fractal analysis applied to characteristic segments of the San Andreas Fault: Journal of Geophysical Research, v. 92, p. 331–344, https://doi.org/10.1029/JB092iB01p00331.

Bilham, R., and Williams, P., 1985, Sawtooth segmentation and deformation processes on the southern San Andreas Fault, California: Geophysical Research Letters, v. 12, p. 557–560, https://doi.org/10.1029/GL012i009p00557.

Byerlee, J., 1978, Friction of rocks, *in* Byerlee, J.D., and Wyss, M., eds., Rock Friction and Earthquake Prediction: Basel, Birkhäuser, p. 615–626, https://doi.org/10.1007/978-3-0348-7182-2_4.

Cambonie, T., Klinger, Y., and Lazarus, V., 2019, Similarities between mode III crack growth patterns and strike-slip faults: Philosophical Transactions of the Royal Society A, v. 377, 20170392, https://doi.org/10.1098/rsta.2017.0392.

Dooley, T.P., and Schreurs, G., 2012, Analogue modelling of intraplate strike-slip tectonics: A review and new experimental results: Tectonophysics, v. 574–575, p. 1–71, https://doi.org/10.1016/j.tecto.2012.05.030.

Hatem, A.E., Cooke, M.L., and Toeneboehn, K., 2017, Strain localization and evolving kinematic efficiency of initiating strike-slip faults within wet kaolin experiments: Journal of Structural Geology, v. 101, p. 96–108, https://doi.org/10.1016/j.jsg.2017.06.011.

King, G., and Nábělek, J., 1985, Role of fault bends in the initiation and termination of earthquake rupture: Science, v. 228, p. 984–987, https://doi.org/10.1126/science.228.4702.984.

Klinger, Y., 2010, Relation between continental strike-slip earthquake segmentation and thickness of the crust: Journal of Geophysical Research, v. 115, B07306, https://doi.org/10.1029/2009JB006550.

Klinger, Y., Xu, X., Tapponnier, P., Van der Woerd, J., Lasserre, C., and King, G., 2005, High-resolution satellite imagery mapping of the surface rupture and slip distribution of the Mw ~7.8, 14 November 2001 Kokoxili earthquake, Kunlun fault, northern Tibet, China: Bulletin of the Seismological Society of America, v. 95, p. 1970–1987, https://doi.org/10.1785/0120040233.

Klinger, Y., Michel, R., and King, G.C.P., 2006, Evidence for an earthquake barrier model from Mw ~7.8 Kokoxili (Tibet) earthquake slip-distribution: Earth and Planetary Science Letters, v. 242, p. 354–364, https://doi.org/10.1016/j.epsl.2005.12.003.

Klinger, Y., et al., 2018, Earthquake damage patterns resolve complex rupture processes: Geophysical Research Letters, v. 45, p. 10,279–10,287, https://doi.org/10.1029/2018GL078842.

Lauer, B., Grandin, R., Klinger, Y., Vallage, A., Jolivet, R., and Delorme, A., 2018, Absence of shallow slip deficit during the Balochistan earthquake (2013, Mw 7.7, Pakistan): Insights from SAR and optical-based coseismic slip model: Abstract T31I-0348 presented at American Geophysical Union Fall Meeting, Washington, D.C., 10–14 December.

Lozos, J.C., 2016, A case for historic joint rupture of the San Andreas and San Jacinto faults: Science Advances, v. 2, e1500621, https://doi.org/10.1126/sciadv.1500621.

Mandl, G., 1987, Discontinuous fault zones: Journal of Structural Geology, v. 9, p. 105–110, https://doi.org/10.1016/0191-8141(87)90047-2.

Manighetti, I., Campillo, M., Bouley, S., and Cotton, F., 2007, Earthquake scaling, fault segmentation, and structural maturity: Earth and Planetary Science Letters, v. 253, p. 429–438, https://doi.org/10.1016/j.epsl.2006.11.004.

Manighetti, I., Caulet, C., De Barros, L., Perrin, C., Cappa, F., and Gaudemer, Y., 2015, Generic along-strike segmentation of Afar normal faults, East Africa: Implications on fault growth and stress heterogeneity on seismogenic fault planes: Geochemistry Geophysics Geosystems, v. 16, p. 443–467, https://doi.org/10.1002/2014GC005691.

Naylor, M.A., Mandl, G., and Supesteijn, C.H.K., 1986, Fault geometries in basement-induced wrench faulting under different initial stress states: Journal of Structural Geology, v. 8, p. 737–752, https://doi.org/10.1016/0191-8141(86)90022-2.

Okubo, P.G., and Aki, K., 1987, Fractal geometry in the San Andreas Fault System: Journal of Geophysical Research, v. 92, p. 345–355, https://doi.org/10.1029/JB092iB01p00345.

Richard, P.D., Naylor, M.A., and Koopman, A., 1995, Experimental models of strike-slip tectonics: Petroleum Geoscience, v. 1, p. 71–80, https://doi.org/10.1144/petgeo.1.1.71.

Riedel, W., 1929, Zur Mechanik geologischer Bruchercheinungen ein Beitrag zum Problem der Fiederspatten: Zentralblatt für Mineralogie, Geologie und Paläontologie Abteilung B, p. 354–368.

Ritter, M.C., Rosenau, M., and Oncken, O., 2018, Growing faults in the lab: Insights into the scale dependence of the fault zone evolution process: Tectonics, v. 37, p. 140–153, https://doi.org/10.1002/2017TC004787.

Rosu, A.-M., Pierrot-Deseilligny, M., Delorme, A., Binet, R., and Klinger, Y., 2015, Measurement of ground displacement from optical satellite image correlation using the free open-source software MicMac: ISPRS Journal of Photogrammetry and Remote Sensing, v. 100, p. 48–59, https://doi.org/10.1016/j.isprsjprs.2014.03.002.

Schwartz, D.P., 2018, Review: Past and future fault rupture lengths in seismic source characterization—The long and short of it: Bulletin of the Seismological Society of America, v. 108, p. 2493–2520, https://doi.org/10.1785/0120160110.

Schwartz, D.P., and Coppersmith, K.J., 1984, Fault behavior and characteristic earthquakes: Examples from the Wasatch and San Andreas fault zones: Journal of Geophysical Research, v. 89, p. 5681–5698, https://doi.org/10.1029/JB089iB07p05681.

Segall, P., and Pollard, D.D., 1980, Mechanics of discontinuous faults: Journal of Geophysical Research, v. 85, p. 4337–4350, https://doi.org/10.1029/JB085iB08p04337.

Tchalenko, J.S., 1970, Similarities between shear zones of different magnitudes: Geological Society of America Bulletin, v. 81, p. 1625–1640, https://doi.org/10.1130/0016-7606(1970)81[1625:SBSZOD]2.0.CO;2.

Ueta, K., Tani, K., and Kato, T., 2000, Computerized X-ray tomography analysis of three-dimensional fault geometries in basement-induced wrench faulting: Engineering Geology, v. 56, p. 197–210, https://doi.org/10.1016/S0013-7952(99)00143-X.

Vallée, M., Landès, M., Shapiro, N.M., and Klinger, Y., 2008, The 14 November 2001 Kokoxili (Tibet) earthquake: High-frequency seismic radiation originating from the transitions between sub-Rayleigh and supershear rupture velocity regimes: Journal of Geophysical Research, v. 113, B07305, https://doi.org/10.1029/2007JB005520.

Wei, S., et al., 2011, Superficial simplicity of the 2010 El Mayor–Cucapah earthquake of Baja California in Mexico: Nature Geoscience, v. 4, p. 615–618, https://doi.org/10.1038/ngeo1213.

Wesnousky, S.G., 2006, Predicting the endpoints of earthquake ruptures: Nature, v. 444, p. 358–360, https://doi.org/10.1038/nature05275.

Yang, H., Moresi, L.N., and Quigley, M., 2020, Fault spacing in continental strike-slip shear zones: Earth and Planetary Science Letters, v. 530, 115906, https://doi.org/10.1016/j.epsl.2019.115906.

Zuza, A.V., Yin, A., Lin, J., and Sun, M., 2017, Spacing and strength of active continental strike-slip faults: Earth and Planetary Science Letters, v. 457, p. 49–62, https://doi.org/10.1016/j.epsl.2016.09.041.

Printed in USA